Sensors and Materials, Vol. 35, No. 3 (2023) 1089–1098
MYU Tokyo

S & M 3231

Optical and Field Emission Properties of Transparent Flexible ZnO Nanowire Films

Wan Shu Cheng,[1] Jiunn Ru Lai,[2] Han Ting Hsueh,[3] and Tsung Chieh Cheng[4*]

[1]Department of Computer Science and Information Management, Providence University, 200, Sec. 7, Taiwan Boulevard, Shalu Dist., Taichung City 43301, Taiwan
[2]Department of Electrical Engineering, National Kaohsiung University of Sciences and Technology, No. 415, Jiangong Rd., Sanmin Dist., Kaohsiung City 807618, Taiwan
[3]Taiwan Semiconductor Research Institute, No. 25, Xiaodong Rd., North Dist., Tainan City 704017, Taiwan
[4]Department of Mechanical Engineering, National Kaohsiung University of Sciences and Technology, No. 415, Jiangong Rd., Sanmin Dist., Kaohsiung City 807618, Taiwan

(Received August 1, 2022; accepted March 8, 2023)

Keywords: ZnO nanowires, flexible substrate, field emitter

Large-area field emitter arrays have important applications in flat-panel displays, light sources, gas sensors, and vacuum pressure sensors, where achieving high field emission currents and current densities over large areas is critical. In this study, well-aligned ZnO nanowires (NWs) were grown on a flexible substrate by the carbothermal reduction process and the vapor–liquid–solid (VLS) method. The ZnO NWs were single-crystalline wurtzite structures that showed a preferential growth orientation along the c-axis. The length and diameter of the ZnO NWs were 0.6 μm and 50 nm, respectively. The experimental results from field emission studies indicated that an emitter constructed from well-aligned, grass-like ZnO NWs exhibited a turn-on field of 16.1 $V\mu m^{-1}$ and a field enhancement factor of $\beta = 1073$, and demonstrated a consistent single linear slope in a Fowler–Nordheim (F–N) plot, which indicates that the field emission from ZnO emitters is a barrier-tunneling, quantum mechanical process. In addition, the field emission properties of curved ZnO/Al-doped ZnO (ZnO/AZO) flexible field nanoemitters were also investigated in this study. The results show that the turn-on field and enhancement factor of ZnO NWs on AZO flexible substrates decrease as the bending angle increases owing to an increase in the total resistance of the AZO layer.

1. Introduction

Advances in research on many vacuum microelectronics devices depend on the realization of reliable high-intensity electron sources. For this reason, the ability to fabricate uniform emitters is an important factor in the application of many sensors and vacuum microelectronics, including their use as electron sources in various visualization equipment, flat-panel displays, electron microscopy, microwave power devices, gas sensors, high-vacuum pressure sensors, and especially in the fabrication of next-generation devices for electron beam lithography.[1–3] Over the past decade, field-emission properties have been studied extensively for various materials

*Corresponding author: e-mail: tcchengme@nkust.edu.tw
https://doi.org/10.18494/SAM4235

ISSN 0914-4935
https://myukk.org/

and geometrical arrangements in which performance has been found to depend strongly on, among other factors, the inherence, morphology, material density, sharpness, aspect ratio, and surface conditions of the tip.[4,5] For a good geometric field enhancement factor, considerable attention has been focused in recent years on the use of one-dimensional (1D) nanotubes or nanowires (NWs) as field emitters. For example, field emission properties of carbon nanotubes (CNTs) have been extensively studied.[6–8] Recently, the advent of new nanofabrication techniques has led to the preparation of efficient electron emitters from various 1D systems comprising different elements — including hollow nanotubes, solid NWs, coaxial cable structures, side-by-side biaxial NWs, and nanobelts — that can deliver highly bright electron beams with a narrow energy spread. Therefore, how to design easy-to-fabricate, low-cost, high-performance field emitters and how to quantitatively understand the physical nature of a single field emitter or an array of field emitters participating in the field-emission process are both very important topics. Field emitters based on other 1D materials such as Si,[9] ZnO,[10] GeO,[11] TiO_2,[12] SnO_2,[13] SiCN,[14] MoO_3,[15] and CuO[16] have also been demonstrated. Among these materials, ZnO is a thermally stable n-type semiconductor with a large exciton binding energy of 60 meV and a large band-gap energy of 3.37 eV at room temperature.[17] ZnO NWs can be synthesized by various methods, such as chemical vapor deposition (CVD),[18] template-assisted growth,[19] catalyst-driven molecular beam epitaxy,[20] the vapor–liquid–solid (VLS) method,[21] and catalyst-free growth by thermal evaporation.[22] However, growth temperatures for these methods are normally higher than 400 °C.

Currently, the devices fabricated on flexible substrates have also attracted much attention. Compared with conventional substrates, flexible substrates are lightweight, thin, bendable, available in large sizes, and low in cost. Flexible substrates are also mass-producible by a roll-to-roll process. To ensure the safety of polymer materials, however, the process temperature for flexible substrates should be limited to 180°C. Instead of high temperatures, it has been shown that ZnO NWs can be synthesized at low temperatures (i.e., <100 °C) by a hydrothermal process.[23,24] Cui *et al.* reported the first growth of ZnO NWs on a flexible plastic substrate by a hydrothermal process.[25] In addition, a ZnO NW-based ethanol gas sensor prepared on a flexible substrate has been demonstrated.[26] In this article, we report the direct growth of high-density ZnO NWs on a flexible substrate and the fabrication of a transparent ZnO NW-based field emitter. We also discuss the physical properties of the ZnO NWs and the electrical properties of the fabricated field emitter.

2. Materials and Methods

The substrate utilized in this study was polyethylene terephthalate (PET). Prior to the growth of ZnO NWs, a PET substrate was cleaned using isopropanol (IPA) and deionized (DI) water. The cleaned substrate was subsequently baked at 100 °C for 10 min to remove any moisture. A 300-nm-thick indium tin oxide (ITO) film was first deposited on the substrate by RF sputtering, after which an 80-nm-thick Al-doped ZnO (AZO) layer was deposited on the substrate by RF sputtering to serve as the seed layer. The ZnO NWs were grown on the AZO substrate by a hydrothermal method. An aqueous solution (80 ml) of 0.02 M $Zn(NO_3)_2$ was mixed with 80 ml

of 0.02 M hexamethylenetetramine (HMT) in a glass vessel. The substrate was immersed in this solution and the vessel was sealed. The sealed vessel was subsequently held in 90 ℃ hot water for 5 h. After the reaction was completed, the resulting white material was poured onto the substrate, which initiated the ZnO film growth. The sample was immediately rinsed in IPA and DI water to remove any residual salt on the surface.

The phase purity and crystallography properties of the samples were examined by X-ray diffraction (XRD) using a MAC MXP18 X-ray diffractometer equipped with monochromatized Cu Kα radiation (λ = 1.541874 Å). The surface morphology and size of the ZnO NWs (NWs) were further observed by field-emission scanning electron microscopy (FESEM, JEOL JSM-7000F), and the transmittance of the ZnO NWs on AZO/PET films was characterized by UV-VIS-NIR spectrophotometery (Varian, Cary 5000). In addition, room-temperature field emission properties of these ZnO NWs grown on a flexible substrate were also investigated in a vacuum chamber at a pressure of 4×10^{-6} Torr. A tungsten probe with a diameter of 1.8 mm was used as the anode, and the distance between the anode and the ZnO NWs was precisely controlled to 50 μm. The bending stage was used to measure the field emission properties of bent ZnO NWs, and the minimum distance between the anode and the ZnO NWs was maintained at 50 nm. A Keithley 237 high-voltage source was used to provide the sweeping electric field and to monitor the emission current for the measurement of field emission properties.

3. Results and Discussion

Figure 1 shows a photograph of the ZnO NWs on a PET substrate with AZO as the seed layer. It is clear that the fabricated sample can be bent easily by hand. Figure 2 shows the top-view and cross-sectional FESEM images of the typical surface morphology of ZnO films prepared by a hydrothermal process. High-density, well-aligned, grass-like ZnO NWs were successfully grown on the top of the AZO/PET substrate. These results also indicate that ZnO NWs consist of densely packed hexagonal grains. The diameters of the ZnO NWs are about 20–120 nm (about

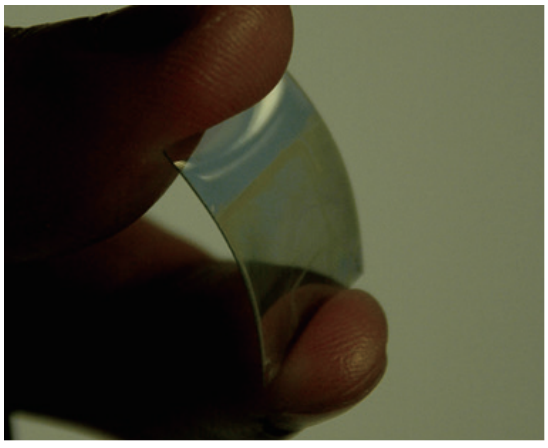

Fig. 1. (Color online) Photograph of a flexible ZnO NW sample.

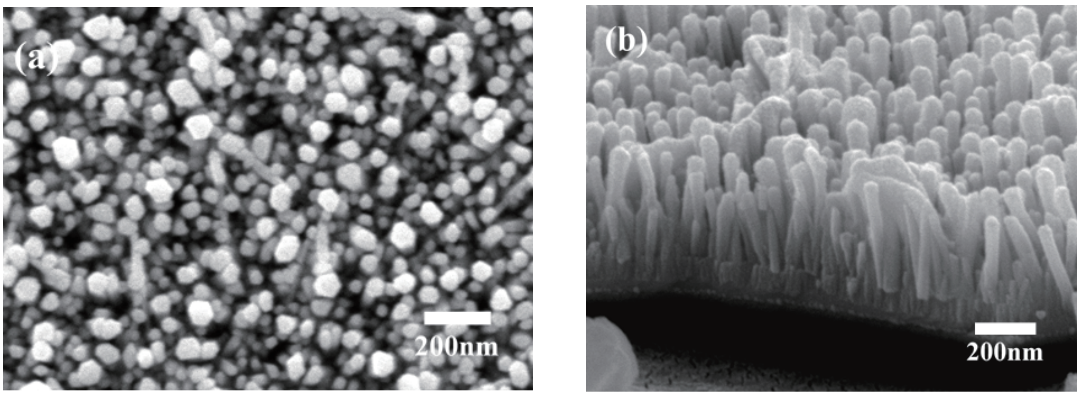

Fig. 2. (a) Top-view and (b) cross-sectional FESEM images of well-aligned ZnO NWs on a flexible AZO/PET substrate.

65 nm on average), and their widths are in the range of 0.2–0.8 μm (about 0.6 μm on average). Figure 3 shows the typical XRD pattern of the as-prepared hydrothermal ZnO NWs. To facilitate the comparison, the XRD spectrum of a bare PET substrate was also recorded and is plotted in Fig. 3. The XRD results indicate that only one strong XRD peak located at $2\theta = 26.06°$ and one shoulder peak located at $2\theta = 22.97°$ were observed from the bare PET substrate. As also shown in Fig. 3, a relatively strong XRD peak located at $2\theta = 34.38°$ and a much weaker XRD peak located at $2\theta = 62.91°$ were observed from the hydrothermally processed sample; these two peaks were associated with ZnO (002) and (103), respectively. The reflections from the XRD results can be indexed to the wurtzite structure of ZnO with lattice parameters $a = 3.247$ Å and $c = 5.20$ Å, in good agreement with the reported data on ZnO (JCPDS File, 5-664). No characteristic peaks from other possible impurities such as $ZnCO_3$ were detected. In addition, compared with the ZnO (103) peak, the significantly stronger ZnO (002) peak suggests that these vertically aligned NWs were preferentially grown along the (002) direction.

Regarding the growth mechanism of the ZnO NWs, it is known that HMT and H_2O can slowly decompose to form NH_3, NH_4^+, and OH^-, while $Zn(NO_3)_2$ can dissociate to form Zn^{2+}.[27]

$$C_6H_{12}N_4 + 6H_2O \rightarrow 4NH_3 + 6HCHO \quad (1)$$

$$H_2O + NH_3 \leftrightarrow OH^- + NH_4^+ \quad (2)$$

$$Zn(NO_3)_2 \rightarrow Zn^{2+} + 2(NO_3)^- \quad (3)$$

Zn^{2+} may then react with NH_3 and OH^- to generate $Zn(OH)_2$ and $Zn(OH)_2(NH_3)_4$. Finally, $Zn(OH)_2$ and $Zn(OH)_2(NH_3)_4$ can be dehydrated to form ZnO.

$$Zn^{2+} + 4NH_3 \leftrightarrow Zn(NH_3)_4^{2+} \quad (4)$$

$$Zn^{2+} + 2OH^- \rightarrow Zn(OH)_2 \quad (5)$$

$$Zn(NH_3)_4^{2+} + 2OH^- \rightarrow Zn(OH)_2(NH_3)_4 \quad (6)$$

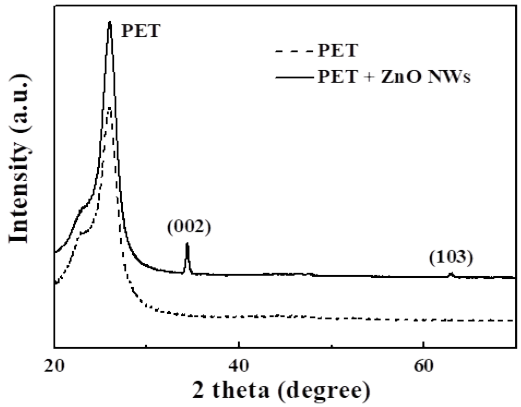

Fig. 3. XRD patterns of ZnO nanowires and PET film.

$$Zn(OH)_2/Zn(OH)_2(NH_3)_4 \rightarrow ZnO + H_2O \tag{7}$$

In this study, to fabricate the flexible ZnO NW-based field emitters, a 300-nm-thick ITO film was first deposited on a PET substrate by RF sputtering. Using four-point resistance measurements, the sheet resistance of the sputtered ITO film was determined to be 180 Ω/□; the film was utilized as the bottom electrode of the field emitter. An 80-nm-thick AZO layer was subsequently deposited on the ITO film as the seed layer, and ZnO NWs were grown on the AZO/ITO/PET substrate by a hydrothermal process. The optical transmittance spectra were recorded using a UV–VIS–NIR spectrophotometer; the results are shown in Fig. 4, which shows the transmittance of the field emitters in the range of 350–800 nm. There was almost zero transmittance (indicated by the total absorption) when the incident wavelength was shorter than 367 nm, and then it increased markedly at longer wavelengths. This fundamental absorption, which corresponds to electron excitation from the valance band to a conduction band, can be used to determine the optical band gap of the ZnO NWs.[28] The relationship between the incident photon energy ($h\nu$) and the transmittance coefficient (T) is shown as

$$\left(\frac{h\nu}{T}\right)^{1/n} = A\left(h\nu - E_g\right), \tag{8}$$

where A is a constant, E_g is the band-gap energy of the material, and the exponent n depends on the type of transition. In this experiment, n is 1/2 for a direct band transition. Therefore, as shown in Fig. 4, the transmittance cut-off wavelength of 367 nm was due to the energy band gap of the ZnO NWs (3.37 eV). The average transmittance was higher than 80% over the range of visible light. Although the flexible substrate has the advantages of low cost, and good flexibility and bendability, it still has the problem of a critical bending angle. Figure 5(a) shows the sample resistance measured in air under various bending angles. The measured resistance changed monotonically when the flexible ZnO NWs/AZO/PET film was bent. As it is bent, the ZnO NWs/AZO layer is squeezed, resulting in a monotonic change in total resistance. The results

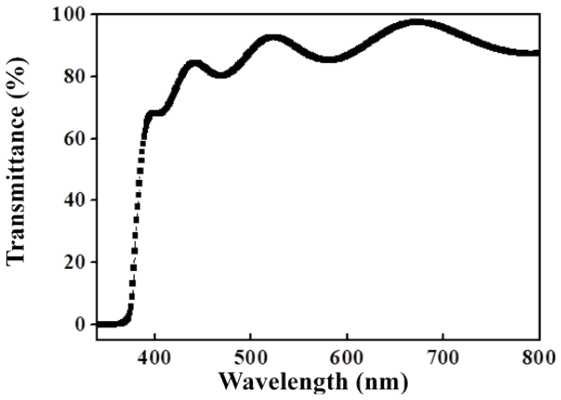

Fig. 4. Transmittance of ZnO nanowire-based field emitters on an AZO/PET substrate.

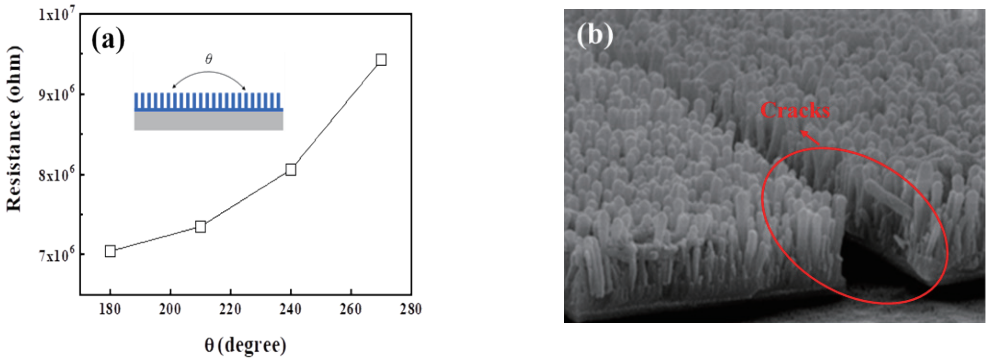

Fig. 5. (Color online) (a) Total resistance of ZnO NWs at different bending angles. (b) SEM image of cracks when the bending angle is larger than 280°.

show that the electrical resistance increases slightly with a decreasing bending diameter (increasing bending angle) owing to the greater bending moment, which increases the propensity of the conductive film to crack and therefore reduces the contact area between the metallic electrodes.[29] In addition, it should be noted that excessive bending can crack the AZO seed layer. According to our experimental results, when the bending angle (θ) is as high as 280 degrees, the conductive transmission line breaks, as shown in Fig. 5(b). The formation of such cracks can cause permanent failure of the device, even if the bending angle is restored to the original state of 180°.

Figure 6 shows the field emission current density–electrical field (J–E) characteristics and Fowler–Nordheim (F–N) plot measured from the fabricated ZnO NW emitters prepared on a flexible substrate. The anode-to-cathode distance was about 50 μm, and voltages from 0 to 1350 V were applied between the anode and the cathode to supply the electric field. The current density J was defined as the total current divided by the sample area. Initially, field emission currents approached zero when the applied field was small, and then the current density showed an exponential dependence on the electric field after a critical point. Without bending the ZnO NW field emitters (θ = 180°), the results indicated that the turn-on field, which is defined as the

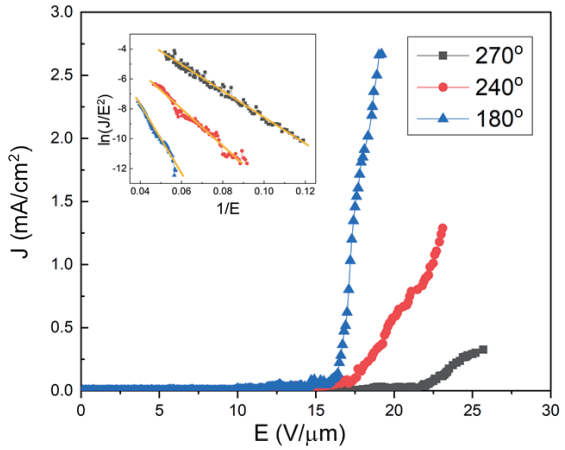

Fig. 6. (Color online) Emission *J*–*E* curves of flexible ZnO NW films at different bending angles. The inset shows the F–N plots of flexible ZnO NW films at different bending angles.

electrical field when the current density becomes 0.1 mA/cm^2, was 16.1 V/mm. The field emission properties of bent, flexible ZnO NW field emitters are shown in Fig. 6. The turn-on fields of the bent samples were 17.6 and 22.7 V/μm at bending angles of 240 and 270°, respectively. These results are in agreement with the data shown in Fig. 5. As the bending angle increased, the total resistance of the ZnO NWs/AZO layer also increased, which directly caused a decrease in the turn-on field of the ZnO NW field emitters. Furthermore, the field emission results also showed that the emission current density measured using the ZnO NWs on a flexible substrate can be fit by the F–N equation,[30]

$$J = A\frac{\beta^2 E^2}{\varnothing}\exp\left(\frac{-B\varnothing^{3/2}}{\beta E}\right), \tag{9}$$

where J is the current density (A/cm^2), E is the applied electric field (V/cm), β is the field enhancement factor, A and B are constants equal to 1.56 × 10^{-6} (A·eV/V^2) and 6.83 × 10^7 (V/cm·eV$^{3/2}$), respectively, and $\varnothing$ (eV) is the work function of ZnO NWs, which is 5.3 eV. Knowing the work function of ZnO NWs, we can further investigate the field emission behavior of the ZnO NWs by replotting ln(J/E^2) as a function of 1/E and taking the logarithm of both sides of Eq. (9),[31] as shown in the inset of Fig. 6:

$$\ln\left(\frac{J}{E^2}\right) = \ln\left(\frac{A\beta^2}{\varnothing}\right) - \frac{B\varnothing^{3/2}}{\beta E}, \tag{10}$$

where A = 1.541434 (μA · eV · V^{-2}) and B = 6.830890 (eV$^{-3/2}$ · Vnm^{-1}). From this F–N plot, the field enhancement factor β was calculated as 1073, 683, and 238 at bending angles of 180, 240, and 270°, respectively. These results also indicated that the field emission properties, such as the turn-on field and the enhancement factor β, became poorer as the bending angle of the flexible

ZnO NW emitter increased. In addition, the F–N curve shown in the inset of Fig. 6 shows a linear relationship between $\ln(J/E^2)$ and $1/E$, indicating that the emitter electron emission follows the field emission mechanism of conventional electron tunneling, which means that the field emission currents originate mainly from the flexible ZnO NWs.

4. Conclusion

High-density well-aligned ZnO NWs were successfully grown on a flexible AZO/PET substrate by a hydrothermal method. With AZO as the seed layer, we grew grass-like ZnO NWs with an average length of 0.6 μm and an average diameter of 65 nm on a PET flexible substrate. Without bending the film of the ZnO NW field emitter, the turn-on field was 16.1 V/mm and the field enhancement factor β was 1073. In addition, increasing the bending angle of a ZnO NW film increases the turn-on field and decreases the enhancement factor owing to increases in both the total resistance of the AZO layer and the anode–cathode distance. A linear F–N curve also indicated that field emission currents were primarily generated from the fabricated ZnO NW emitters. Consequently, the well-aligned and grass-like ZnO NWs obtained by a hydrothermal method without using any catalyst are promising emitter sources for use in flexible electronic sensors and device applications.

Acknowledgments

The authors thank the National Science and Technology Council of the Republic of China, Taiwan, for supporting this research under Contract No. NSTC 111-2221-E-992-060-MY2.

References

1 B. K. Gupta, G. Kedawat, P. Kumar, S. Singh, S. R. Suryawanshi, N. Agrawal, G. Gupta, A. R. Kim, R. K. Gupta, M. A. More, D. J. Late, and M. G. Hahm: RSC Adv. **6** (2016) 9932. https://doi.org/10.1039/C5RA25682H
2 W. P. Kang, Y. M. Wong, J. L. Davidson, D. V. Kerns, B. K. Choi, and K. F. Galloway: IEEE Electron Lett. **42** (2006) 210. https://doi.org/10.1049/el:20064239
3 B. K. Gupta, G. Kedawat, A. K. Gangwar, K. Nagpal, P. K. Kashyap, S. Srivastava, S. Singh, P. Kumar, S. R. Suryawanshi, D. M. Seo, P. Tripathi, M. A. More, O. N. Srivastava, M. G. Hahm, and D. J. Late: AIP Adv. **8** (2018) 015117. https://doi.org/10.1063/1.5004769
4 L. Chen, H. Yu, J. Zhong, J. Wu, and W. Su: J. Alloys Compd. **749** (2018) 60. https://doi.org/10.1016/j.jallcom.2018.03.100
5 J. Singh and A. Srivastava: Mater. Sci. Semicond. **138** (2022) 106282. https://doi.org/10.1016/j.mssp.2021.106282
6 S. Iijima: Nature **354** (1991) 56. https://www.nature.com/articles/354056a0
7 Y. K. Ko, J. Geng, S. G. Jang, S. M. Yang, T. W. Jeong, Y. W. Jin, J. M. Kim, and H. T. Jung: Carbon **47** (2009) 1555. https://doi.org/10.1016/j.carbon.2009.02.001
8 P. Gabdullin, A. Zhurkin, V. Osipov, N. Besedina, O. Kvashenkina, and A. Arkhipov: Diamond Relat. Mater. **105** (2020) 107805. https://doi.org/10.1016/j.diamond.2020.107805
9 H. T. Hsueh, T. J. Hsueh, S. J. Chang, F. Y. Hung, C. L. Hu, W. Y. Weng, C. W. Liu, Y. H. Lee, and B. T. Dai: Electrochem. Solid-State Lett. **13** (2010) K29. https://doi.org/10.1149/1.3290776
10 E. Rauwel, A. Galeckas, M. Rosário Soares, and P. Rauwel: J. Phys. Chem. C **121** (2017) 14879. https://doi.org/10.1021/acs.jpcc.7b03070
11 Z. G. Bai, D. P. Yu, H. Z. Zhang, Y. Ding, X. Z. Gai, Q. L. Hang, G. C. Xiong, and S. Q. Feng: Chem. Phys. Lett. **303** (1999) 311. https://doi.org/10.1016/S0009-2614(99)00066-4

12 Q. Zhang, L. Ma, M. Shao, J. Huang, M. Ding, X. Deng, X. Wei, and X. Xu: J. Nanomater. **2014** (2014) 831752. https://doi.org/10.1155/2014/831752
13 L. A. Ma, Z. H. Wei, X. Y. Ye, J. Y. Lin, L. Q. Hu, and T. L. Guo: Ceram. Int. **43** (2017) 6096. https://doi.org/10.1016/j.ceramint.2017.02.002
14 F. G. Tarntair, C. Y. Wen, L. C. Chen, J.-J. Wu, K. H. Chen, P. F. Kuo, S. W. Chang, Y. F. Chen, W. K. Hong, and H. C. Cheng: Appl. Phys. Lett. **76** (2000) 2630. https://doi.org/10.1063/1.126431
15 Y. B. Li, Y. Bando, D. Golberg, and K. Kurashima: Appl. Phys. Lett. **81** (2002) 3648. https://doi.org/10.1063/1.1738174
16 T. H. Chang, C. Y. Hsu, H. C. Lin, K. H. Chang, and Y. Y. Li: J. Alloys Compd. **644** (2015) 324. https://doi.org/10.1016/j.jallcom.2015.04.107
17 N. Kumar, A. Dorfman, and J. Hahm: J. Nanosci. Nanotechnol. **5** (2005) 1915. https://doi.org/10.1166/jnn.2005.422
18 R. Bhujel, S. Rai, and B. P. Swain: Mater. Sci. Semicond. Process. **102** (2019) 104592. https://doi.org/10.1016/j.mssp.2019.104592
19 Y. Li, G. W. Meng, L. D. Zhang, and F. Phillipp: Appl. Phys. Lett. **76** (2000) 2011. https://doi.org/10.1063/1.126238
20 Y. W. Heo, V. Varadarajan, M. Kaufman, K. Kim, D. P. Norton, F. Ren, and P. H. Fleming: Appl. Phys. Lett. **81** (2002) 3046. https://doi.org/10.1063/1.1512829
21 C. L. Hsu, S. J. Chang, H. C. Hung, Y. R. Lin, C. J. Huang, Y. K. Tseng, and I. C. Chen: IEEE Tran. Nanotechnol. **4** (2005) 649. https://doi.org/10.1109/TNANO.2005.851394
22 T. J. Hsueh, S. J. Chang, Y. R. Lin, S. Y. Tsai, I. C. Chen, and C. L. Hsu: Cryst. Growth Des. **6** (2006) 1282. https://doi.org/10.1021/cg060188j
23 L. Vayssieres: Adv. Mater. **15** (2003) 464. https://doi.org/10.1002/adma.200390108
24 L. E. Greene, M. Law, J. Goldberger, F. Kim, J. D. Johnson, Y. F. Zhang, R. J. Saykally, and P. D. Yang: Angew. Chem. Int. Ed. **42** (2003) 3031. https://doi.org/10.1002/ange.200351461
25 J. B. Cui, C. P. Daghlian, U. J. Gibson, R. Püsche, P. Geithner, and L. Ley: J. Appl. Phys. **97** (2005) 044315. https://doi.org/10.1063/1.1854206
26 H. Ahn, J. H. Park, S. B. Kim, S. H. Jee, Y. S. Yoon, and D. J. Kim: Electrochem. Solid-State Lett. **13** (2010) J125. https://doi.org/10.1149/1.3479692
27 X. Yan, Z. Li, R. Chen, and W. Gao: Cryst. Growth. Des. **8** (2008) 2406. https://doi.org/10.1021/jp908101z
28 C. S. Pathak, D. D. Mishra, V. Agarwala, and M. K. Mandal: Ceram. Int. **38** (2012) 5497. https://doi.org/10.1016/j.ceramint.2012.03.063
29 G. Saggio, F. Riillo, L. Sbernini, and L. R. Quitadamo: Smart Mater. Struct. **25** (2016) 013001. https://doi.org/10.1088/0964-1726/25/1/013001
30 R. H. Fowler and L. W. Nordheim: Proc. R. Soc. London, Ser. A **119** (1928) 173. https://doi.org/10.1098/rspa.1928.0091
31 W. Li, M. Zhang, and Z. Li: Mater. Chem. Phys. **277** (2022) 125631. https://doi.org/10.1016/j.matchemphys.2021.125631

About the Authors

Wan Shu Cheng received her Ph.D. degree from the Department of Computer Science and Information Engineering, National Cheng Kung University, Taiwan, in 2014. She was an assistant professor in the Department of Electrical Engineering at National Kaohsiung University of Science and Technology and in the Department of Computer Science and Information Management at Providence University in 2019 and 2022, respectively. Her current research interests include data mining and its applications, sensor technologies, computer vision, big data analysis, and precision medicine. (iqn.ws.cheng@gmail.com)

Jiunn Ru Lai received his B.S., M.S. and Ph.D. degrees from Taiwan University, Taipei, Taiwan in 1995, 1997 and 2004, respectively. From 2006 to 2015, he was an assistant professor at National Kaohsiung University of Applied Science, Taiwan. Since 2015, he has been an associate professor at National Kaohsiung University of Science and Technology. His research interests are in sensors, wireless network, and embedded systems. (jrlai@mail.ee.nkust.edu.tw)

Han Ting Hsueh received his Ph.D. degree from National Cheng Kung University, Taiwan, in 2012. He is now a division director of the Heterogeneous Integration and Manufacturing Division at Taiwan Semiconductor Research Institute, National Applied Research Laboratories. He has many years of experience in the design, nanofabrication, and integration of MEMS and sensors. His current research interests cover the range of advanced packages, including 2.5D/3D fabrication, sensors, and AIOT heterogeneous integration.

Tsung Chieh Cheng received his Ph.D. degree from the Department of Mechanical Engineering, National Chiao Tung University in 2002. From 2002 to 2004, he worked at the Tainan Division of the National Nano Devices Laboratory (NDL) as an associated researcher. In 2005, he was promoted to the material characteristic division in Hsinchu NDL. Since 2016, he has been a professor at National Kaohsiung University of Science and Technology. His research interests are in surface modification, semiconductor materials, and sensors. (tcchengme@nkust.edu.tw)